https://doi.org/10.48048/tis.2023.5890

Effect of Salt Content and Operating Temperature on the Nitrogen Dioxide Gas Sensing Performance of Sodium-Ion Conducting Solid Polymer Electrolyte

Saja Neama Kareem[1], Mahdi Hasan Suhail[1] and Omed Gh. Abdullah[2,*]

[1]Department of Physics, College of Science, University of Baghdad, Baghdad 10001, Iraq
[2]Advanced Materials Research Laboratory, Department of Physics, College of Science, University of Sulaimani, Sulaymaniyah 46001, Iraq

([*]Corresponding author's e-mail: omed.abdullah@univsul.edu.iq)

Received: 7 September 2022, Revised: 1 October 2022, Accepted: 7 October 2022, Published: 2 June 2023

Abstract

Sodium-ion conducting solid polymer electrolyte (Na-SPE) films based on polyvinyl alcohol (PVA) with various weight percentages of sodium iodide (NaI) were prepared using the casting technique. The films' structural, morphology and electrical conductivity were examined to understand the sensing mechanism of the as-prepared Na-SPE films. The X-ray diffraction (XRD) and atomic force microscopy (AFM) data, respectively, showed the amorphous and homogeneous granular structure of Na-SPE films due to the high dissociation of NaI in the PVA matrix for all concentrations. The changes in the FTIR vibrational modes of Na-SPEs provide evidence of interactions between cations and functional groups of the host matrix. The effect of salt content, operating temperature and gas concentration on the performance of the Na-SPE sensor towards NO_2 were investigated. In contrast to the pure PVA film, which did not respond to NO_2 gas at low concentrations, Na-SPE films exhibit higher sensitivity to NO_2 gas with faster response and recovery times. At low NO_2 gas concentration (50 ppm), a sample containing 20 wt.% of NaI exhibits the highest sensitivity at the operating temperature of 200 °C. In comparison, at a high NO_2 gas concentration (550 ppm), a sample containing 40 wt.% of NaI exhibits a maximum sensitivity at 150 °C. These findings suggest that Na-SPE films would be suitable for gas sensor applications.

Keywords: Conductivity, Gas sensing, Operating temperature, Sodium-ion conducting, Sensitivity

Introduction

The environmental monitoring of atmospheric gas pollutants in urban areas has received much attention from researchers due to their adverse impacts on human health and the environment [1,2]. Automobiles, agriculture, industry and household activities produce most of these gas pollutants [3]. One of the main air quality issues to be concerned about is the reddish-brown gas known as nitrogen dioxide (NO_2). Both natural and human activities, including those associated with power plant activities, car engines and heating, all contribute to the release of NO_2 into the atmosphere [4-7]. Exposure to NO_2 can affect human health even at the ppb level. Therefore, fast detection and accurate monitoring of this toxic gas have become essential in our daily life [8]. Conventional solid-state metal oxide semiconductor-based gas sensors are inexpensive and highly sensitive. However, their performance still suffers from poor selectivity, lack of long-term stability and high operating temperatures (total power consumption) [9-11]. As a result, developing next-generation high-performance gas sensors to detect NO_2 with desirable properties, including high sensitivity, low detection limit and fast response/recovery times at low operating temperature, is crucially important for both health protection and environmental [12,13].

Considerable attention has been paid to polymers in a blend or composite form as novel materials for potential applications in gas sensors, biosensors, capacitors and electronic devices [14,15]. Since their electrical conductivity can alter when exposed to oxidizing or reducing gas molecules, they have considerable promise as chemical gas sensors [16]. Due to their great sensitivity and quick response times at room temperature, organic conducting polymers, such as polyaniline (Pani), polypyrrole (PPy) and their derivatives, have been extensively used as the active layers of gas sensors. Additionally, polymeric materials have good mechanical properties, which allow a facile fabrication of sensors [17]. One of the most promising materials for high-performance gas sensors is organic-inorganic hybrid material because

of its improved properties like high sensitivity, selectivity, quick response/recovery times, adaptability and low power consumption [18,19].

Among all synthetic polymers, polyvinyl alcohol (PVA) films, both doped and undoped, have been the subject of numerous studies due to their wide range of industrial applications and inexpensive cost. PVA has a particular chemical potential to create electrolytes due to its hydrophilic properties and the large number of hydroxyl groups connected to the methane carbons on the PVA backbone [20]. Jiang *et al.* [21] examine the sensing characteristics of PPy/PVA blend as gas sensors produced by continuous vapor state polymerization technique. They observed an increase in sensitivity by incorporating PVA into the PPy upon exposure to methanol gas, while the response and recovery times were worse. Zhang *et al.* [22] studied proton-conducting solid-state electrolytes based on PVA as an electrochemical gas sensor for the detection of alcohol. The prepared membranes have low ethanol detection limits of 25 ppm and excellent sensitivity.

In this study, the sensing properties of Na-SPE films based on PVA incorporating varying weight percentages of NaI were investigated. The sensitivity, response time, and recovery time of the sensors towards NO_2 gas were systematically studied. The investigation of films' structural, morphology and electrical properties is to understand the mechanism of the sensing process to further enhance the system's sensitivity. The focus of this study is to investigate the effect of NaI salt content, operating temperature, and NO_2 concentration on gas sensing performance towards NO_2 gas.

Materials and methods

Polyvinyl alcohol (PVA) powder (M.W. = 14,000 g/mol, degree of hydrolysis 87 - 89 %) supplied by Central Drug House Ltd., and sodium monoiodide (NaI) salt (M.W. = 149.894 g/mol) provided by Merck, were used to synthesize sodium-ion conducting solid polymer electrolyte (Na-SPE) with varying salt contents (10, 20, 30 and 40 wt.% of NaI). An aqueous solution of the polymer host matrix was prepared by dissolving 2.5 g of PVA powder in 100 mL of double distilled water on a hot plate at 80 °C with constant stirring for 2 h. The final clear solution was cooled to room temperature. A required amount of NaI was added to every 10 mL of transparent PVA solution under stirring for 20 min to ensure complete mixing. To obtain a transparent solid layer of Na-SPEs with a uniform thickness, the homogeneously mixed solutions were cast onto a glass substrate, the entire assembly was placed in a dust-free chamber, and the solvent was allowed to slowly evaporate in the air at room temperature for 3 days. The average thickness of the prepared Na-SPE films is equal to 0.2 - 0.3 µm. The SPE films were designated 10Na-SPE, 20Na-SPE, 30Na-SPE and 40Na-SPE for PVA incorporated 10, 20, 30 and 40 wt.% of NaI, respectively. Then, the films were stored in a desiccator containing anhydrous silica gel to avoid the influence of humidity before being characterized.

The X-ray diffraction (XRD) patterns for the prepared Na-SPE films were obtained by using Bruker D8 Adv. Diffractometer instrument with CuK_α target having the wavelength λ = 1.5418 Å. Atomic force microscope (AFM) model AA3000 was employed to monitor the surface morphology for Na-SPE films, using parameters such as average roughness, root-mean-square roughness, grain size and particle size distribution. Fourier transform infrared (FTIR) spectroscopy was performed by a Bruker Alpha Corporation in the wavenumber region between 400 and 4,000 cm^{-1} to analyze the change in the bond structure of the host matrix upon the formation of Na-SPE films. A computer-controlled measurement system was used to carry out the Hall-effect experiment. The gas sensor has been designed to measure the resistance change of Na-SPE films in air and gaseous atmosphere using a Keithley electrometer model 6514, with 6 V bias voltages. The films were put in a 250 mL sealed container to monitor the films' response, and a syringe was used to inject NO_2 gas. All the sensing measurements were conducted at varying operating temperatures (150, 200, 250 and 300 °C) and different NO_2 gas concentrations of 50 and 550 ppm. The resistance of the films was recorded before and after exposure to the NO_2 gas. The sensitivity (S) is characterized by $S = (R_g - R_a)/R_a \times 100$ %, where R_a and R_g, respectively, the sensor's resistance in ambient air and test gas. The times taken by the sensor to achieve 90 % of the total resistance change on exposure to gas and air are, respectively, defined as the response and recovery times.

Results and discussion

Figure 1 displays the XRD patterns for pure PVA and Na-SPE films. The diffraction pattern of pure film exhibits a broad band at 2θ = 19.25 °, demonstrating the semi-crystalline nature of PVA, which is caused by intermolecular hydrogen bond interactions due to the proximity of the hydroxyl (-OH) groups [23]. The XRD patterns of Na-SPEs show a broadening in the PVA characteristic band and a decrease in the diffraction intensity, both of which point to the predominance of the amorphous phase. This could be due to disrupting the PVA's semi-crystalline phase by adding NaI salt [24,25]. The absence of crystalline

peaks of the salt in the SPEs indicates that the NaI has entirely dissolved in the matrix due to its low lattice energy [26,27]. The high dissociation of NaI in the PVA matrix results in a rise in the free charge carriers, and an increase in the amorphous domain leads to flexibility in the polymer backbone, resulting in better ionic diffusivity through the matrix, which improves the ion conductivity of the SPE system [28-31].

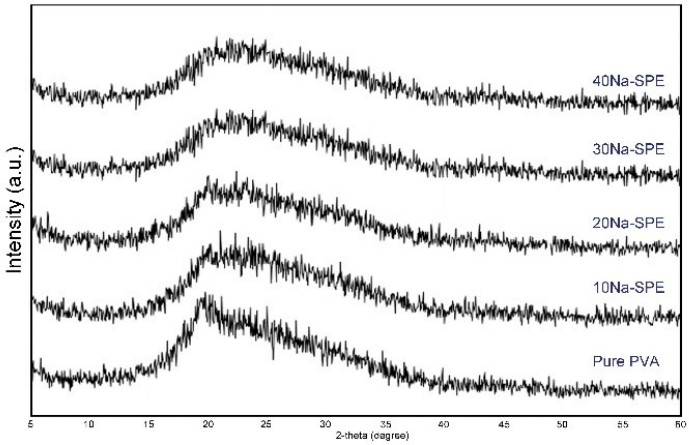

Figure 1 The XRD patterns for pure PVA and Na-SPE films.

It has been well reported that the sensing performance of gas sensors is greatly affected by the surface morphology of the thin films. The sensor sensitivity increases linearly with an increase in the effective surface area of thin films [32]. Therefore, Atomic-force microscopy (AFM) was used to examine the surface morphology of as-prepared Na-SPEs with different NaI contents. In the 3D images of the surfaces presented in **Figure 2**, all films display a granular structure almost uniformly dispersed on a surface free of cracks. The sensitivity of gas sensors is directly correlated with the film roughness. The granular films exhibit high gas-sensing sensitivity because they have a higher surface area for film-gas interaction [33,34].

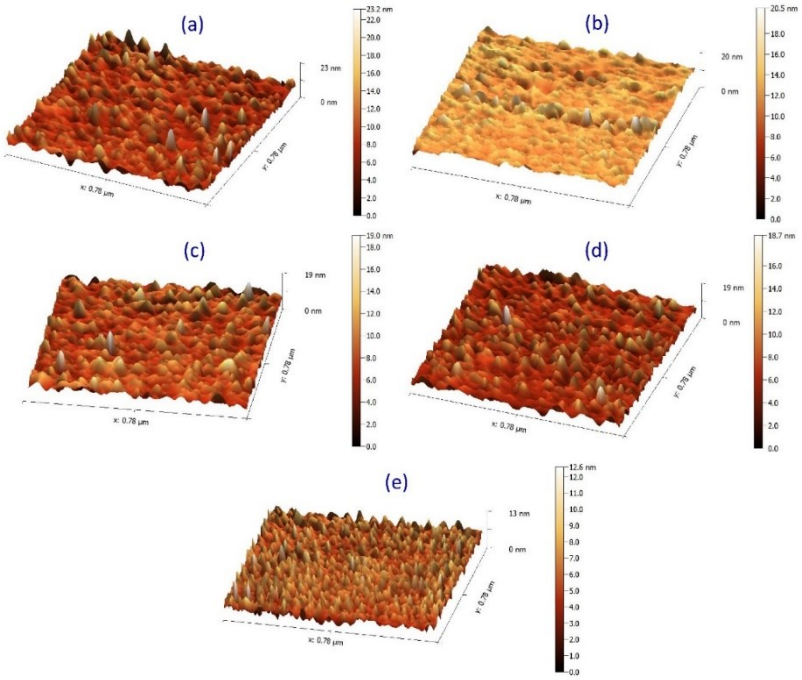

Figure 2 AFM images for pure PVA and Na-SPE films at different NaI percentages.

The main parameters inferred from AFM images, including root mean square, average roughness and particle size of the randomly distributed particles, are affected by NaI content, as shown in **Figure 3**. The surface roughness of the films can be attributed to the grain growth of different sizes. The high surface

roughness of pure PVA sample designates a highly gas sensitivity of this polymer. In addition, the 20Na-SPE sample has the largest particle size. This sample is therefore expected to have better gas sensing performance than other samples, including pure PVA.

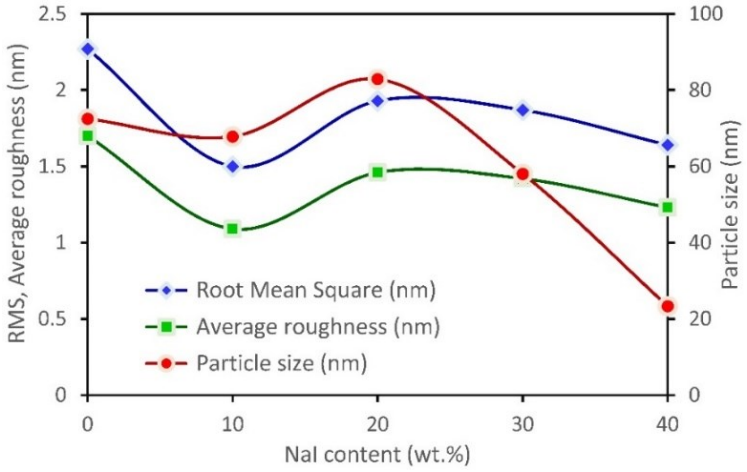

Figure 3 AFM parameters for pure PVA and Na-SPE films at different NaI percentages.

Figure 4 depicts the FTIR spectra in transmittance mode for pure PVA and 40Na-SPE films. The spectrum of pure PVA film exhibits several discrete bands of stretching and bending vibrations of the functional groups, consistent with earlier studies [35,36]. The prominent peaks of PVA were observed at 3,434, 2,917, 1,637, 1,412, 1,098, 799 and 640 cm^{-1}. These peaks are assigned, respectively, to the OH stretching vibration of the hydroxyl group, CH_2 asymmetric stretching vibration, C=O carbonyl stretching, C-H bending vibration of CH_2, C-O stretching vibrations of acetyl groups, C-C stretching vibration and C-H out-of-phase bending, accordingly [37,38].

The FTIR spectrum of the 40Na-SPE film also exhibits the characterized bands of pure PVA. When NaI salt is added to the PVA matrix, there is a noticeable shift in band positions as well as a slight change in some band intensities, both of which indicate structural changes in the complex. For example, the O-H stretching band for SPE film is shifted to 3,410 cm^{-1}, C-H stretching band shifted to 2,920 cm^{-1} and the C-O stretching vibrations appeared at 1,060 cm^{-1}. Nevertheless, the addition of NaI to the PVA matrix caused changes in the vibration wavenumbers of some bands. The spectrum of the 40Na-SPE film does not contain any recognizable NaI salt peaks. This demonstrates the complexation of salt with polymer [39]. Thus the observed frequency shifts of the PVA bands after adding NaI salt caused the structure changes as a result of interaction and complexation between dissociated salt and matrix [40]. This result is consistent with the XRD analysis.

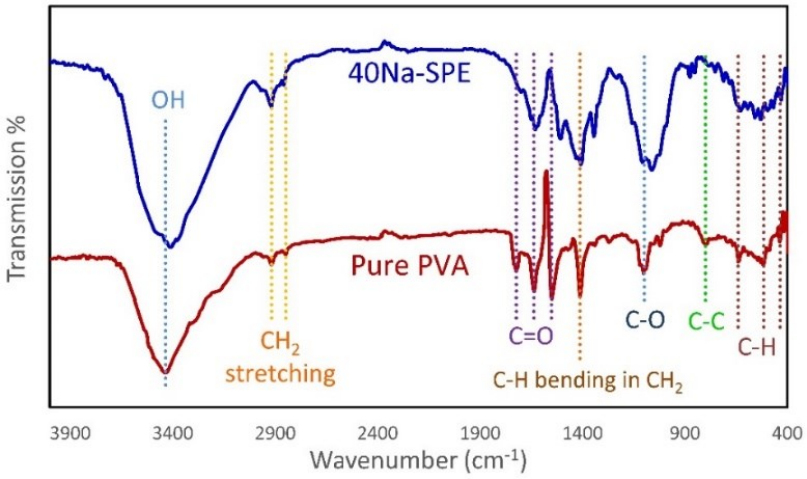

Figure 4 FTIR patterns for pure PVA and 40Na-SPE films.

The room temperature Hall effect parameters such as carrier concentration, conductivity and carrier mobility for pure PVA and Na-SPE films have been determined in this study. The Hall coefficient signal for Na-SPE films is negative, indicating that the carriers in this compound are n-type [41,42]. The carrier concentration (n), conductivity (σ) and carrier mobility (μ) were calculated, and the values are arranged in **Table 1**. According to the Hall effect measurement, incorporating NaI to the PVA matrix increases conductivity and carrier density of SPE up to 20 wt.% and decreases with further increase of salt content. Thus this sample (20Na-SPE) has minimum resistivity (i.e., the maximum change in resistivity); it will show the highest gas sensitivity, as seen later.

Table 1 Hall effect parameters for pure PVA and Na-SPEs with different NaI percentages.

Samples	$n \times 10^{16}$ (cm^{-3})	σ ($\Omega \cdot cm^{-1}$	μ (cm^2/V_s)
Pure PVA	4.52	19.9	2,740
10Na-SPE	4.13	20.3	3,070
20Na-SPE	6.15	21.3	2,160
30Na-SPE	5.56	20.2	2,270
40Na-SPE	5.65	20.1	2,220

The effectiveness of a sensor can be determined by its sensitivity, reaction time, and recovery time. Response and recovery times were defined as the required time by the sensor to reach 90 % of the maximum response when gas is injected and 10 % when gas is removed, respectively [43]. To test the sensitivity of the samples to detect a low concentration of NO_2 gas, 50 ppm of NO_2 gas was injected over the Na-SPE films at different operating temperatures of 150, 200, 250 and 300 °C. The pure PVA film has not exhibited any sensitivity to the examined gas at this low gas concentration. It turns out that when a sensor is exposed to NO_2 gas, its conductivity value increases and its resistance decreases. The resistance rises to its initial value when the gas is turned off. As a result, the gas sensing mechanism of membranes depends on the adsorption or interaction of NO_2 gas molecules on their surface. [27,44]. **Figures 5(a)** - **5(c)** represents the temperature dependence of sensitivity, response time and recovery time for Na-SPE films at various weight percentages of 10, 20, 30 and 40 % and under the same ambient conditions. The 20Na-SPE film exhibits the highest sensitivity to NO_2 gas at a temperature of 200 °C compared to other concentrations. The reduced surface area with possible reaction sites on the film's surface may cause a decreased response time [45-47].

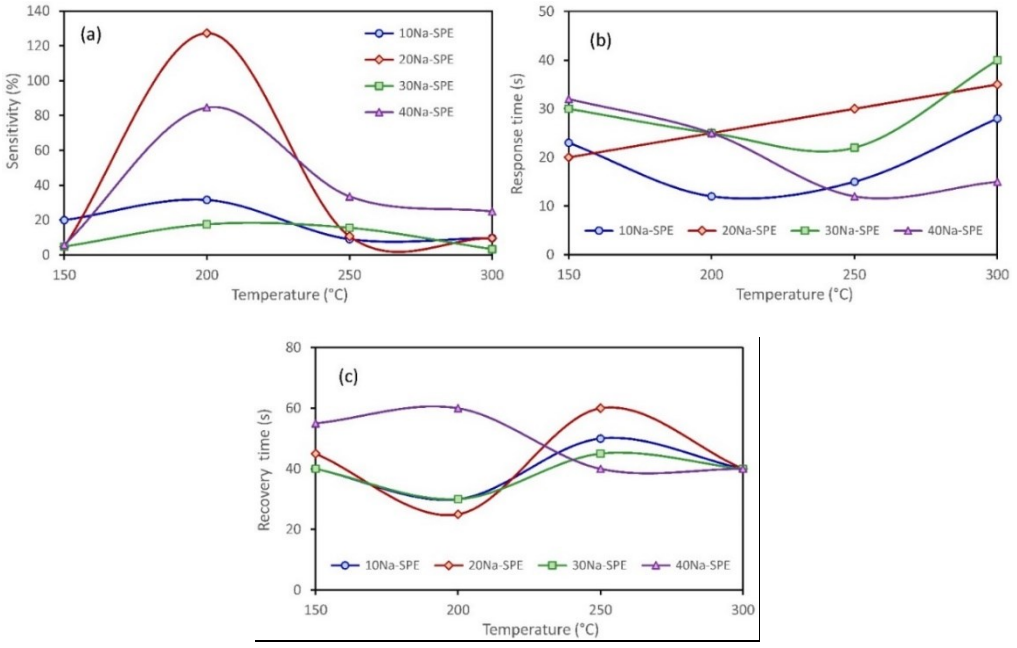

Figure 5 Temperature dependence of NO_2 gas (a) sensitivity, (b) response time, and (c) recovery time for Na-SPE films at various weight percentages of NaI.

The 20Na-SPE film shows a strong response to NO_2 gas with rapid reaction and short recovery time at a temperature of 200 °C with a high sensitivity of 127.3 %. According to AFM test results shown in **Figure 3**, the increase in surface roughness and particle size is the cause of the maximum sensitivity of the 20Na-SPE film at low NO_2 gas concentration.

To test the NO_2 gas sensitivity of Na-SPEs at high gas concentrations, 550 ppm of NO_2 gas was injected over the sensors of pure PVA and Na-SPEs at varying operating temperatures. **Figure 6** shows the resistance change as a function of time for PVA thin film examined under exposure to 550 ppm NO_2 gas at operating temperatures 50, 100 and 150 °C. The data of the resistance variation over time were used to determine response and recovery times when exposed to 550 ppm NO_2 gas at various operating temperatures, as depicted in **Figure 6**. This calculation is based on the phenomenon that gas molecules adsorbing or desorbing on the surface of a sensor changes the resistance of the device [48].

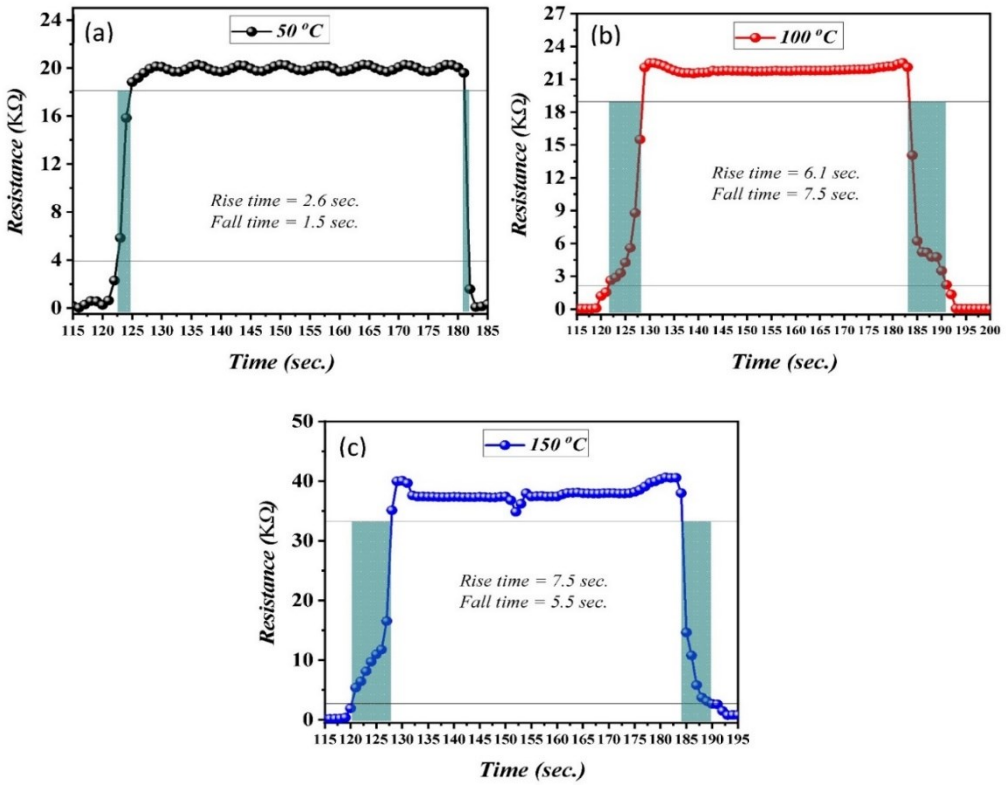

Figure 6 Resistance change of PVA thin film examined under exposure to 550 ppm NO_2 gas at operating temperatures (a) 50 °C, (b) 100 °C, and (c) 150 °C.

Figures 7(a) - 7(b) represents the resistance variation over time for Na-SPE films at various weight percentages of 10, 20, 30 and 40 %, respectively. It can be noted in these figures that the electrical resistance values for all SPE samples continuously increase with increasing NaI content. The time-dependent resistance curves were used to determine sensitivity, response time, and recovery time for all as-deposited Na-SPE films exposed to 550 ppm NO_2 gas at various operating temperatures.

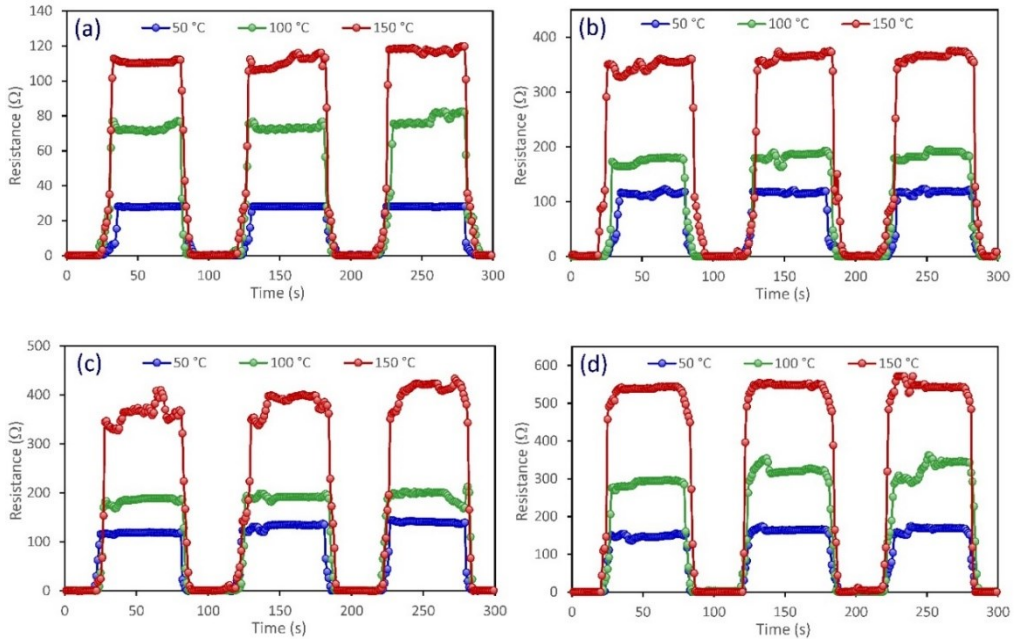

Figure 7 Resistance change of (a) 10Na-SPE, (b) 20Na-SPE, (c) 30Na-SPE, and (d) 40Na-SPE thin films, examined under exposure to 550 ppm NO_2 gas at different operating temperatures.

Figure 8 represents sensitivity, response time and recovery time as a function of temperature for pure PVA and Na-SPE films at various weight percentages of NaI (10, 20, 30 and 40 wt.%) when exposed to 550 ppm NO_2 under the same ambient conditions. The best response time of the sensors towards NO_2 gas was found at a working temperature of 150 °C for a 40Na-SPE at a concentration of 550 ppm and was about 2.5 s, while the recovery time was about 5 s. It is also evident that this sample exhibits the maximum sensitivity of 126 % to NO_2 gas in the same condition. The sensor's response time depends on how quickly gas molecules diffuse and react with the active layer of SPEs. Thus the 2 factors that affect sensor response are the rate of chemical reaction on the surface grain and the spreading speed of gas molecules on this surface [49].

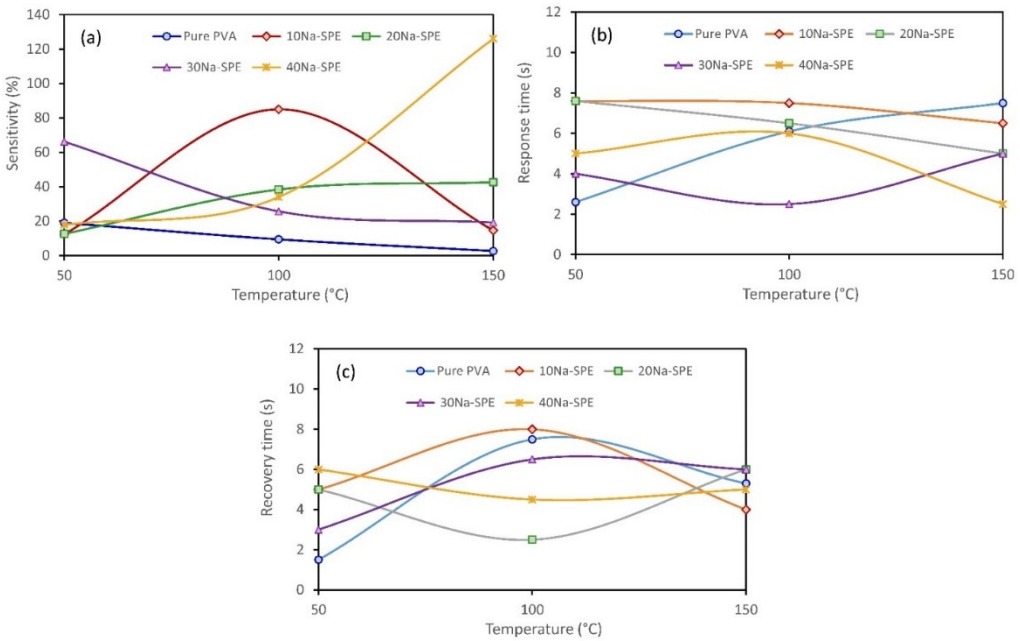

Figure 8 Temperature dependence of NO_2 gas (a) sensitivity, (b) response time, and (c) recovery time for pure PVA and Na-SPE films at various weight percentages of NaI.

The sensing materials and the type of gases to be analyzed determine the optimum operating temperature, which may be caused by a change in the gas molecule adsorption and desorption rates on the sensing element's surface [50]. The maximum sensor response occurs at 150 °C and is caused by an increase in the rate of NO_2 molecules interacting with the sensing surface, which may be mostly the result of improvements in the rate of adsorption rather than desorption [51]. These results suggest that Na-SPE films would be suitable for commercial and environmental sensor applications.

Conclusions

The casting method has been used to produce Na-SPEs films based on PVA with varying salt amounts. The study was focused on investigating the effect of NaI salt content, operating temperature and NO_2 concentration on gas sensing performance towards NO_2 gas. The structural, morphology and electrical conductivity of the Na-SPE films were investigated to understand the detailed sensing mechanism of the compound. The Hall effect data confirm the n-type conductivity of the Na-SPEs. The pure PVA film did not indicate any response to NO_2 gas at a low concentration. However, the Na-SPE structure exhibits high sensitivity with rapid response/recovery times, which are essential features for sensor applications. At low NO_2 gas concentration, 20Na-SPE film shows the maximum sensitivity of 127.3 % at a temperature of 200 °C, while at high gas concentration, the maximum sensitivity of 126 % was achieved for 40Na-SPE at 150 °C. These results imply that this compound would suit environmental and industrial uses.

Acknowledgements

The authors gratefully acknowledge the assistance and lab facilities provided by the Department of Physics, College of Science at the University of Baghdad, Iraq.

References

[1] SW Lee, W Lee, Y Hong, G Lee and DS Yoon. Recent advances in carbon material-based NO_2 gas sensors. *Sensor. Actuator. B Chem.* 2018; **255**, 1788-804.

[2] AC Catto, LF da Silva, MIB Bernardi, S Bernardini, K Aguir, E Longo and VR Mastelaro. Local structure and surface properties of $Co_xZn_{1-x}O$ thin films for ozone gas sensing. *ACS Appl. Mater. Interfac.* 2016; **8**, 26066-72.

[3] S Dhall, BR Mehta, AK Tyagi and K Sood. A review on environmental gas sensors: Materials and technologies. *Sensor. Int.* 2021; **2**, 100116.

[4] M Virghileanu, I Savulescu, BA Mihai, C Nistor and R Dobre. Nitrogen dioxide (NO_2) pollution monitoring with sentinel-5P satellite imagery over Europe during the coronavirus pandemic outbreak. *Rem. Sens.* 2020; **12**, 3575.

[5] CT Lee, HY Lee and YS Chiu. Performance improvement of nitrogen oxide gas sensors using Au catalytic metal on SnO_2/WO_3 complex nanoparticle sensing layer. *IEEE Sensor. J.* 2016; **16**, 7581-5.

[6] VC Nguyen, K Kim and H Kim. Performance optimization of nitrogen dioxide gas sensor based on Pd-AlGaN/GaN HEMTs by gate bias modulation. *Micromachines* 2021; **12**, 400.

[7] İA Resitoglu, K Altinisik and A Keskin. The pollutant emissions from diesel-engine vehicles and exhaust aftertreatment systems. *Clean Tech. Environ. Pol.* 2015; **17**, 15-27.

[8] X Yan, Y Wu, R Li, C Shi, R Moro, Y Ma and L Ma. High-performance UV-assisted NO_2 sensor based on chemical vapor deposition graphene at room temperature. *ACS Omega* 2019; **4**, 14179-87.

[9] X Sun, J Yang, Z Wu, G Meng, X Guo, D Kuang, L Xiong, W Qu, X Fang, X Yang, X Tang and Y He. Lead-free $CsCu_2I_3$ perovskite nanostructured networks gas sensor for selective detection of trace nitrogen dioxide at room temperature. *IEEE Sensor. J.* 2021; **21**, 14677-84.

[10] MA Patil, VV Ganbavle, KY Rajpure, HP Deshmukh and SH Mujawar. Fast response and highly selective nitrogen dioxide gas sensor based on zinc stannate thin films. *Mater. Sci. Energ. Tech.* 2020; **3**, 36-42.

[11] P Raju and Q Li. Review - semiconductor materials and devices for gas sensors. *J. Electrochem. Soc.* 2022; **169**, 057518.

[12] L Guo, YW Hao, PL Li, JF Song, RZ Yang, XY Fu, SY Xie, J Zhao and YL Zhang. Improved NO_2 gas sensing properties of graphene oxide reduced by two-beam-laser interference. *Sci. Rep.* 2018; **8**, 4918.

[13] A Shakeel, K Rizwan, U Farooq, S Iqbale and AA Altaff. Advanced polymeric/inorganic nanohybrids: An integrated platform for gas sensing applications. *Chemosphere* 2022; **294**, 133772.

[14] JC Bittencourt, BHS Gois, VJRD Oliveira, DLS Agostini and CA Olivati. Gas sensor for ammonia detection based on poly(vinyl alcohol) and polyaniline electrospun. *J. Appl. Polymer Sci.* **2019**; 136, 47288.
[15] Y Hu, H Yu, Z Yan and Q Ke. The surface chemical composition effect of a polyacrylic acid/polyvinyl alcohol nanofiber/quartz crystal microbalance sensor on ammonia sensing behavior. *RSC Adv.* 2018; **8**, 8747-54.
[16] Y Yan, G Yang, JL Xu, M Zhang, CC Kuo and SD Wang. Conducting polymer-inorganic nanocomposite based gas sensors: A review. *Sci. Tech. Adv. Mater.* 2020; **21**, 768-86.
[17] YC Wong, BC Ang, ASMA Haseeb, AA Baharuddin and YH Won. Conducting polymers as chemiresistive gas sensing materials: A review. *J. Electrochem. Soc.* 2020; **167**, 037503.
[18] W Hittini, YE Greish, NN Qamhieh, MA Alnaqbi, D Zeze and ST Mahmoud. Ultrasensitive and low temperature gas sensor based on electrospun organic-inorganic nanofibers. *Org. Electron.* 2020; **81**, 105659.
[19] N Singha, S Neogi, B Pramanik, S Das, A Dasgupta, R Ghosh and D Das. Ultrafast, highly sensitive, and selective detection of p-xylene at room temperature by peptide-hydrogel-based composite material. *ACS Appl. Polymer Mater.* 2019; **9**, 2267-72.
[20] T Remis, P Belsky, T Kovarik, J Kadlec, MG Azar, R Medlin, V Vavrunkova, K Deshmukh and KK Sadasivuni. Study on structure, thermal behavior, and viscoelastic properties of nanodiamond-reinforced poly (vinyl alcohol) nanocomposites. *Polymers* 2021; **13**, 1426.
[21] L Jiang, HK Jun, YS Hoh, JO Lim, DD Lee and JS Huh. Sensing characteristics of polypyrrole-poly(vinyl alcohol) methanol sensors prepared by in situ vapor state polymerization. *Sensor. Actuator. B Chem.* 2005; **105**, 132-7.
[22] J Zhang, G Jiang, T Cumberland, P Xu, Y Wu, S Delaat, A Yu and Z Chen. A highly sensitive breathable fuel cell gas sensor with nanocomposite solid electrolyte. *InfoMat* 2019; **1**, 234-41.
[23] OG Abdullah. Synthesis of single-phase zinc chromite nano-spinel embedded in polyvinyl alcohol films and its effects on energy band gap. *J. Mater. Sci. Mater. Electron.* 2016; **27**, 12106-11.
[24] T Siddaiah, P Ojha, NO Gopal, C Ramu and H Nagabhushana. Thermal, structural, optical and electrical properties of PVA/MAA: EA polymer blend filled with different concentrations of Lithium Perchlorate. *J. Sci. Adv. Mater. Dev.* 2018; **3**, 456-63.
[25] KL Chai, MM Aung, IM Noor, HN Lim and LC Abdullah. Observation of ionic conductivity on PUA-TBAI-I_2 gel polymer electrolyte. *Sci. Rep.* 2022; **12**, 124.
[26] PB Bhargav, VM Mohan, AK Sharma and VVRN Rao. Structural and electrical studies of sodium iodide doped poly(vinyl alcohol) polymer electrolyte films for their application in electrochemical cells. *Ionics* 2007; **13**, 173-8.
[27] VM Mohan, V Raja, AK Sharma and VVRN Rao. Ionic conductivity and discharge characteristics of solid-state battery based on novel polymer electrolyte (PEO+$NaBiF_4$). *Mater. Chem. Phys.* 2005; **94**, 177-81.
[28] A Poosapati, E Jang, D Madan, N Jang, L Hu and Y Lan. Cellulose hydrogel as a flexible gel electrolyte layer. *MRS Comm.* 2019; **9**, 122-8.
[29] V Cyriac, Ismayil, IM Noor, K Mishra, C Chavan, RF Bhajantri and SP Masti. Ionic conductivity enhancement of PVA: Carboxymethyl cellulose poly-blend electrolyte films through the doping of NaI salt. *Cellulose* 2022; **29**, 3271-91.
[30] TSRT Naiwi, MM Aung, M Rayung, A Ahmad, KL Chai, MLW Fui, EZM Tarmizi and NAA Aziz. Dielectric and ionic transport properties of bio-based polyurethane acrylate solid polymer electrolyte for application in electrochemical devices. *Polymer Test.* 2022; **106**, 107459.
[31] Q Yang, A Wang, J Luo and W Tang. Improving ionic conductivity of polymer-based solid electrolytes for lithium metal batteries. *Chin. J. Chem. Eng.* 2022; **43**, 202-15.
[32] Y Shen, T Yamazaki, Z Liu, D Meng, T Kikuta and N Nakatani. Influence of effective surface area on gas sensing properties of WO_3 sputtered thin films. *Thin Solid Films* 2009; **517**, 2069-72.
[33] NG Deshpande, YG Gudage, R Sharma, JC Vyas, JB Kim and YP Lee. Studies on tin oxide-intercalated polyaniline nanocomposite for ammonia gas sensing applications. *Sensor. Actuator. B Chem.* 2009; **138**, 76-84.
[34] MH Suhail, IK Adehmash, SMA Kareem, DA Tahir and OG Abdullah. Construction of Cr_2O_3:ZnO nanostructured thin film prepared by pulsed laser deposition technique for NO_2 gas sensor. *Trans. Electr. Electron. Mater.* 2020; **21**, 355-65.
[35] HM Zidan, EM Abdelrazek, AM Abdelghany and AE Tarabiah. Characterization and some physical studies of PVA/PVP filled with MWCNTs. *J. Mater. Res. Tech.* 2019; **8**, 904-13.

[36] SM Pawde, K Deshmukh and S Parab. Preparation and characterization of poly(vinyl alcohol) and gelatin blend films. *J. Appl. Polymer Sci.* 2008; **109**, 1328-37.
[37] A Kharazmi, N Faraji, RM Hussin, E Saion, WMM Yunus and K Behzad. Structural, optical, opto-thermal and thermal properties of ZnS-PVA nanofluids synthesized through a radiolytic approach. *Beilstein J. Nanotechnology* 2015; **6**, 529-39.
[38] I Omkaram, RPS Chakradhar and JL Rao. EPR, optical, infrared and Raman studies of VO^{2+} ions in polyvinylalcohol films. *Phys. B Condens. Matter.* 2007; **388**, 318-25.
[39] N Kulshrestha, B Chatterjee and PN Gupta. Structural, thermal, electrical, and dielectric properties of synthesized nanocomposite solid polymer electrolytes. *High Perform. Polymer.* 2014; **26**, 677-88.
[40] MO Farea, AM Abdelghany, MS Meikhail and AH Oraby. Effect of cesium bromide on the structural, optical, thermal and electrical properties of polyvinyl alcohol and polyethylene oxide. *J. Mater. Res. Tech.* 2020; **9**, 1530-8.
[41] MH Suhail, AA Ramadan, SB Aziz and OG Abdullah. Chemical surface treatment with toluene to enhances sensitivity of NO_2 gas sensor based on CuPcTs/Alq_3 thin films. *J. Sci. Adv. Mater. Dev.* 2017; **2**, 301-8.
[42] MH Suhail, OG Abdullah and GA Kadhim. Hydrogen sulfide sensors based on PANI/f-SWCNT polymer nanocomposite thin films prepared by electrochemical polymerization. *J. Sci. Adv. Mater. Dev.* 2019; **4**, 143-9.
[43] W Chen, Q Zhou, F Wan and T Gao. Gas sensing properties and mechanism of nano-SnO_2-based sensor for hydrogen and carbon monoxide. *J. Nanomaterials* 2012; **2012**, 612420.
[44] FJ Hameed, IM Ibrahim, OG Abdullah and MH Suhai. Enhancing optical and electrical gas sensing properties of polypyrrole nanoplate by dispersing nano-sized tungsten oxide. *ECS J. Solid State Sci. Tech*. 2021; **10**, 107001.
[45] NT Thang, LT Hong, NH Thoan, CM Hung, NV Duy, NV Hieu and ND Hoa. Controlled synthesis of ultrathin MoS_2 nanoflowers for highly enhanced NO_2 sensing at room temperature. *RSC Adv.* 2020; **10**, 12759-71.
[46] TP Mokoena, HC Swart, KT Hillie, ZP Tshabalala, M Jozela, J Tshilongo and DE Motaung. Enhanced propanol gas sensing performance of p-type NiO gas sensor induced by exceptionally large surface area and crystallinity. *Appl. Surf. Sci.* 2022; **571**, 151121.
[47] BG Ghule, SF Shaikh, NM Shinde, SS Sangale, PV Shinde and RS Mane. Promoted room-temperature LPG gas sensor activities of graphene oxide@Fe_2O_3 composite sensor over individuals. *Mater. Res. Express* 2018; **5**, 125001.
[48] A Afzal, N Cioffi, L Sabbatini and L Torsi. NO_x sensors based on semiconducting metal oxide nanostructures: Progress and perspectives. *Sensor. Actuator. B Chem.* 2012; **171-172**, 25-42.
[49] J Guo, W Li, X Zhao, H Hu, M Wang, Y Luo, D Xie, Y Zhang and H Zhu. Highly sensitive, selective, flexible and scalable room-temperature NO_2 gas sensor based on hollow SnO_2/ZnO nanofibers. *Molecules* 2021; **26**, 6475.
[50] AB Khatibani and M Abbasi. Comparison of gas sensing properties of spray pyrolysed VO_x thin films. *J. Mater. Sci. Mater. Electron.* 2015; **26**, 5052-9.
[51] A Alagh, FE Annanouch, KA Youssef, C Bittencourt, F Guell, PR Martinez-Alanis, M Reguant and E Llobet. PdO and PtO loaded WS_2 boosts NO_2 gas sensing characteristics at room temperature. *Sensor. Actuator. B Chem.* 2022; **364**, 131905.